Efficient metasurface for electromagnetic energy harvesting with high capture efficiency and a wide range of incident angles

Abdulrahman Ahmed Ghaleb Amer, Syarfa Zahirah Sapuan & Adel Y. I. Ashyap

Published online: 29 Sep 2022.

Submit your article to this journal ⟋

Article views: 90

View related articles ⟋

View Crossmark data ⟋

Taylor & Francis
Taylor & Francis Group

Check for updates

Efficient metasurface for electromagnetic energy harvesting with high capture efficiency and a wide range of incident angles

Abdulrahman Ahmed Ghaleb Amer [a], Syarfa Zahirah Sapuan[a] and Adel Y. I. Ashyap[b]

[a]Faculty of Electrical and Electronic Engineering, Universiti Tun Hussein Onn Malaysia (UTHM), Batu Pahat, Malaysia; [b]Faculty of Engineering Technology, Universiti Tun Hussein Onn Malaysia (UTHM), Johor, Malaysia

ABSTRACT

This work introduces a miniaturized metasurface (MS) energy harvester operating at 5.54 GHz with a high capture efficiency and a wide incident angle. The proposed MS structure is comprised of an ensemble of electric ring resonator (ERR) array. The MS's impedance is engineered to match free space, so that the incident electromagnetic (EM) power is efficiently captured with minimal reflection and delivered to the optimal resistor load through an optimally positioned metallic-via. According to the simulation results obtained by CST Microwave Studio, the proposed MS harvester achieves higher conversion efficiency of about 91% under normal incidence and more than 78% across a wider incident angle up to 60°. In order to verify the simulation results, a 5×5 cell array of the proposed MS harvester is fabricated and tested. The simulation and experimental results are well match. The proposed MS configuration can be attractive for high-efficiency and compact wireless sensor network harvesting systems.

1. Introduction

The wireless power transfer (WPT) technique has been received much attention in a variety of applications, including wireless sensor networks (WSN), and the internet of things (IoT) [1,2]. There are two types of WPT based on radiation fields and the coupling of evanescent fields: far-field WPT and near-field WPT [3]. The far-field WPT, which uses a rectenna device, is frequently referred to as RF energy harvesting (RFEH). The WSN technology is applied in various applications in environmental [3], industrial [4], health monitoring [5], security [6], N-park monitoring, etc. However, the power supply of the sensor node is a major challenge facing WSN technologies. Batteries, which have a limited lifespan, are still the primary power source for the sensor nodes. However, large sensor node deployments require frequent battery replacement, which is inefficient and costly. In

CONTACT Abdulrahman Ahmed Ghaleb Amer ✉ aag2014ye@gmail.com 🖃 Faculty of Electrical and Electronic Engineering, Universiti Tun Hussein Onn Malaysia (UTHM), Batu Pahat 86400, Malaysia; Syarfa Zahirah Sapuan
✉ syarfa@uthm.edu.my Faculty of Electrical and Electronic Engineering, Universiti Tun Hussein Onn Malaysia (UTHM), Batu Pahat 86400, Malaysia

order to overcome the issue mentioned above, the RFEH system is the best technique that could be implemented to power the sensors.

The concept of RFEH is to absorb the EM waves energy from the environment and deliver it to the load. The primary device in an RFEH system is the rectenna, which is comprised of three parts: a receiving antenna, a matching network, and a rectifier circuit [7]. The use of conventional antenna arrays as RFEH collectors (receiving antennas) is limited by the antennas' large dimensions, the distance between them in array form, and low power conversion efficiency due to the mutual coupling between the array elements [8–10]. A promising alternative to conventional antennas, MS structures have recently been used in the RFEH system to reduce the overall collector's size and increase the efficiency of converting RF radiation into AC power [11,12]. The MS structures are often defined as two-dimensional counterparts of metamaterial that show interesting EM manipulations not found in normal material. The MS structures have wide applications due to their unique wave manipulation capabilities, including EM energy absorbers [13,14], polarization manipulation [15], cloaking, and imaging [16]. Several MS structures for RFEH have been studied in the recent literature [12]. In particular, a MS energy harvester based on split-ring resonator (SRR) and complementary split-ring resonator (CSRR) were investigated [17–19]. In addition, the MS with the characteristics of a wide-angle reception of incident angles [20–22], multiband [23, 24], and polarization-insensitive [25–28] were investigated.

This paper presents a simple MS structure as an energy harvester in the microwave regime. The operation frequency of 5.54 GHz was chosen partly because it is included in the Industrial, scientific, and medical (ISM) frequency band. The proposed MS structure is a miniaturized cross-shaped resonator hosted on a thin grounded dielectric substrate and mounted by a resistive load. The proposed MS harvester effectively absorbs incident EM power and delivers it to a resistive load through a metallic via positioned optimally. The proposed MS harvester was designed and analyzed using the commercially available CST Microwave Studio. The harvester is achieved a higher conversion efficiency of more than 90% under normal incidence and about 78% at an oblique incidence up to 60°.

2. Design of the MS harvester

In the light of the paper's objective of developing a wide-angle MS harvester, the simplest type of the electric-ring resonators (ERRs), namely, the cross-shaped resonator, is considered. The evaluation of this objective leads to the construction of the MS structure depicted in Figure 1.

The proposed MS unit cell consists of cross shaped resonator covered with a thin dielectric Rogers RO4350B having dielectric constant, $\varepsilon_r = 3.66$, tangent loss of $\delta = 0.0037$, and thickness of 1.524 mm. A full copper layer serves as a ground plane on the backside, effectively blocking transients. The dielectric substrate was chosen for its low loss, preventing absorbed power from dissipating. The geometrical parameters of the proposed MS unit cell shown in Figure 1(a), were as follow (dimensions in mm) the periodicity of the cell, $P = 12$ mm, length of the metallic resonator, $L1 = 11.4$ mm, a width of the metallic resonator, $W1 = 4$ mm, length of the slot, $L2 = 7.6$ mm, a width of the slot, $W2 = 1.2$ mm, and the spacing between adjacent unit cells, $S = 0.3$ mm. The metallic resonator on the top layer is connected to the ground plane by a matching resistor element through a via/probe.
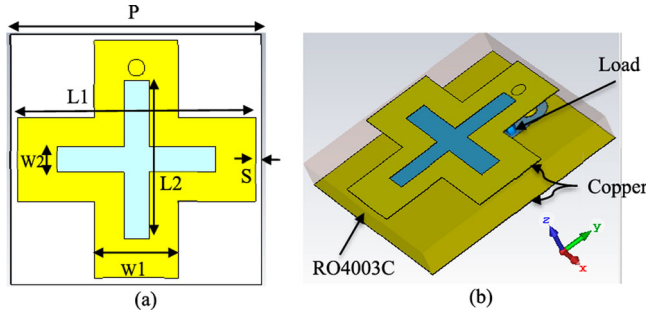
Figure 1. Geometry of the MS structure: (a) Top view and (b) perspective view.

The resistive load is crucial for optimizing the absorption and harvesting efficiencies. CST sweeping revealed that the optimal absorption and harvesting efficiencies occur when the resistance is 50 Ω at the operating frequency. It is important to note that the optimized resistance value (50 Ω) is primarily influenced by the unit cell's size and topology, the properties of the substrate, and the position of the via. All numerical simulations for this study were done in CST Microwave Studio. An infinite unit cell simulation was required to improve computing efficiency during the design development stage. However, due to the difficulty of creating an infinite array, a unit cell in the center of a large array may conduct similarly to an infinite array's unit cell. As a result, an infinitely periodic structure along the x-y axes of a unit cell was simulated using the periodic boundary condition. The Floquet ports predict an incident wave propagating in the z-direction to excite the proposed unit cell using two orthogonally polarized plane waves usually propagating to the xy-plane.

3. Results and discussion

The most important indicator for a harvester is harvesting efficiency, defined as an energy harvester's capturing energy by the footprint area and delivering the maximum absorbed power to the load [17]. This study aims to maximize harvesting efficiency at a wide range of incidence angles. The radiation to AC conversion efficiency was calculated by

$$\eta_{Rad \to AC} = P_{load}/P_{incident} \tag{1}$$

where, the $P_{incident}$ represents the total time average power incident on the footprint area and P_{load} represents the total time average power dissipated on the load and can be described by

$$P_{load} = \sum_{n=1}^{N} V_i^2/R_i \tag{2}$$

where, V_i is the voltage across the ith MS collector's resistance R_i and N the total number of MS collectors.
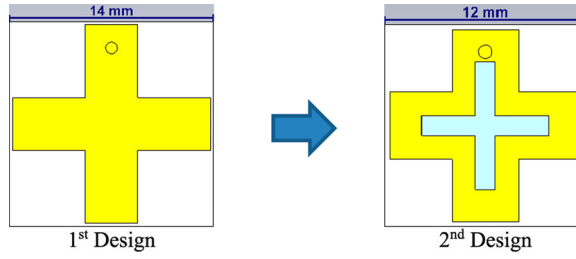
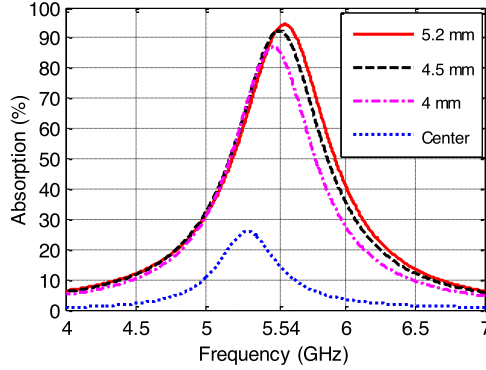**Figure 2.** Unit cell improvement for the optimal performance.

Figure 3. Dependence of the absorption response on the via position away from the resonator center.

3.1. Simulated results

To optimize the proposed MS harvester unit cell's performance, the unit cell design was evolved as shown in Figure 2. The cross-slot was incorporated into the resonator's patch to reduce the unit cell's size (2nd Design).

First, using the 1st design, the numerical investigation of the effect of via hole position away from the resonator's center on the absorption ratio is carried out as shown in Figure 3. The absorption ratio can be calculated as

$$A(\omega) = 1 - |S_{11}(\omega)|^2 - |S_{21}(\omega)|^2 \tag{3}$$

where $S_{11}(\omega)$ and $S_{21}(\omega)$ are the reflection and transmission coefficients, respectively. Since the full ground plane, the transmission is almost zero. Thus, the absorption ratio is expressed as

$$A(\omega) = 1 - |S_{11}(\omega)|^2 \tag{4}$$

It has been observed that increasing the distance between the via position and the resonator center increases the absorption response. In Figure 3, the absorption response of more than 94% is achieved at a distance of 5.2 mm from the resonator center, demonstrating the effectiveness of the design.

In order to investigate the effect of the cross-slot on the performance of the MS harvester, the cross-slot length, defined as *L2* in Figure 1 is varied from 6 mm to 7.4 mm in the step
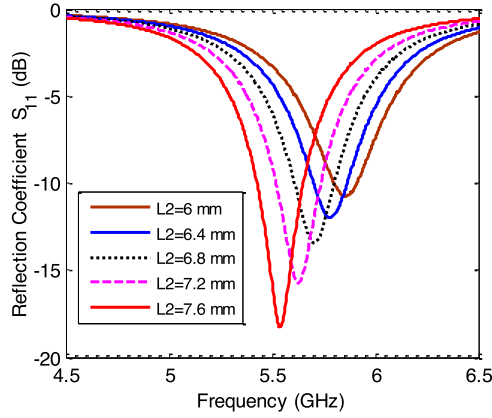
Figure 4. Dependence reflection coefficient $|S_{11}|$ on cross-slot length.
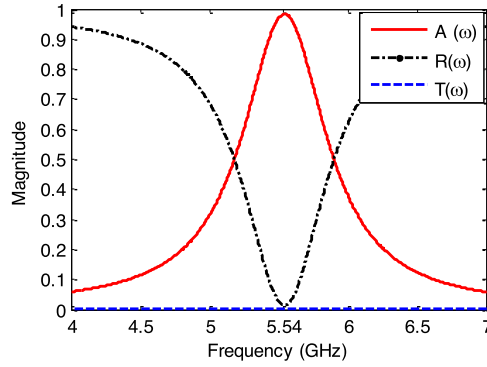

Figure 5. Absorption and reflection coefficients under normal incidence.

of 0.4 mm while all other parameters are kept constant. Figure 4 shows the reflection coefficient with the $L2$ varied from 6 mm to 7.4 mm. It is clear that the resonance frequency shifts to the lower side as the $L2$ varies. This can be explained based on the equation of $f = 1/2\pi\sqrt{LC}$ which indicates that as capacitance and inductance values change, the resonance frequency changes as well. Based on this investigation, the chosen value is $L2 = 7.6$ mm has an acceptable reflection coefficient ($< 18\ dB$) at 5.54 GHz, as depicted in Figure 4.

After a thorough evaluation of the designs, 2nd design is chosen as the final design for the proposed MS harvester and numerically investigated to demonstrate its performance in absorbing and delivering EM power into the load. Figure 5 depicts the absorption, reflection and transmission coefficients under normal incidence. As shown in Figure 5, a near-unity absorption of more than 98% is obtained at the operating frequency of 5.54 GHz.

The surface currents distribution is investigated and analysed in order to evaluate the performance of the proposed MS harvester. The top metallic layer's surface current distribution was anti-parallel, resulting in current loops and a high magnetic resonance with the
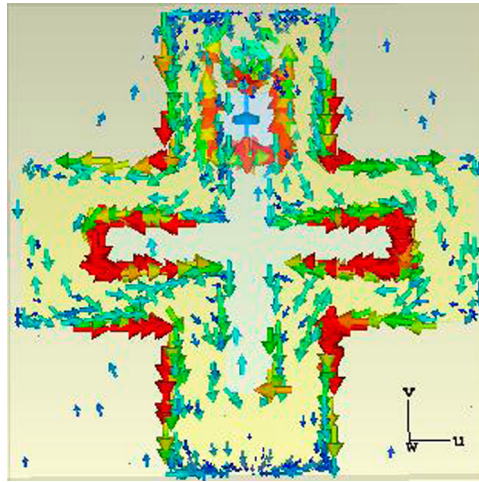
Figure 6. Simulated surface current distribution.

MS structure. The structure's overlapping magnetic and electric resonances were responsible for the high EM absorption. The surface current is distributed throughout the MS structure, with higher concentrations along the y-axis on the top side of the cross-resonator and along the x-axis on the left and right edges of the cross-slot (See Figure 1). The maximum surface current density is delivered to the load by placing the via hole on the top side of the resonator (along the y-axis), as shown in Figure 6.

Some factors were critical in transferring the absorbed power to the resistor load. To begin, a low-loss substrate with a low-loss tangent is used. Besides that, the effective via hole location directs the maximum density of the resonator's current surface to the resistive load through the via/probe. Numerical simulations were investigated to study power distribution into the cell by calculating power loss in the lumped resistor, Rogers's dielectric substrate, and copper. As shown in Figure 7, the power accepted by the cell was around 98%. The power of 91% and 7% are dissipated across resistor load, and the dielectric substrate and copper, respectively. This maximum power delivery to the load was primarily achieved by using a low loss substrate and, more importantly, the resistive load value corresponding to the MS structure's input impedance.

For the practical EM environment, the direction and polarization of the EM wave are unknown. As a result, the MS harvester with a wide range of angular stability is desirable. The proposed MS harvester was investigated in order to determine its ability to capture incoming radiation from various incident angles. The MS harvester was computed at different incident angles from 0° to 75° in the step of 15°. Figure 8 shows the absorption ratio for the proposed harvester at various incident angles where the polarization angles is $\varphi = 0^\circ$. An absorption ratio of about 98.3%, 98.7%, 99%, and 96.5% are achieved at the incident angles of 0°, 15°, 30°, and 45° at 5.54 GHz, respectively. When the incident angle increased to 60° and 75°, an absorption ratio of about 91% and 69.3% are achieved at 5.59 and 5.6 GHz, respectively, as depicted in Figure 8. Angle stability is caused by the presence
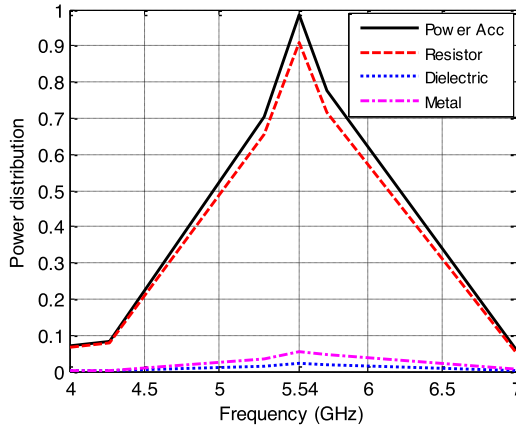
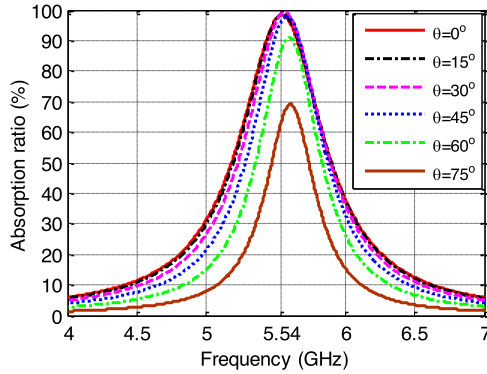**Figure 7.** Power distribution within the cell.

Figure 8. Absorption ratio at different incident angles.

of a metallic ground plane and via in this type of structure [29, 30]. A decrease in absorption value with increasing incident angle is due to the change in the direction of the EM incident wave and a decrease in the incident magnetic flux on the MS structure.

Figure 9 shows the absorption ratio at different polarization angles (ϕ) from 0° up to 450° where the incident angles is constant at $\theta = 0^o$. The proposed MS harvester is a polarization-insensitive up to 450°. As shown in Figure 9, with increase of the polarization angle the absorption ratio is decreased.

The microwave to AC conversion efficiency is the critical figure of merit for energy harvesting. It is defined as the average power dissipated on a load to the average power incident. CST Microwave Studio is used to calculate the power losses into the proposed MS unit cell. The microwave to AC efficiency is evaluated using an Equation (1). Figure 10 shows the radiation to AC efficiency at different oblique incident angles from 0° up to 60° in the step of 150°. When the incident angle is $\theta = 0^o$ and $\theta = 15^o$ the maximum radiation to AC efficiency of about 91%, and 87.2% are achieved at 5.54 and 5.47 GHz, respectively. For the incident angle $\theta = 30^o$ and $\theta = 45^o$, the radiation to AC efficiency of about 90% was achieved at 5.51 and 5.6 GHz, respectively. For $\theta = 60^o$, the maximum efficiency of about 78.2% was achieved at 5.67 GHz. It was noticed that as the incident angle increases, the
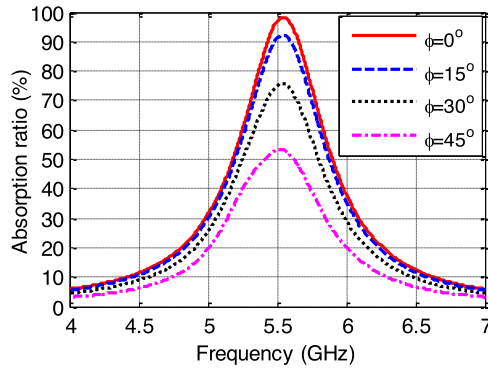
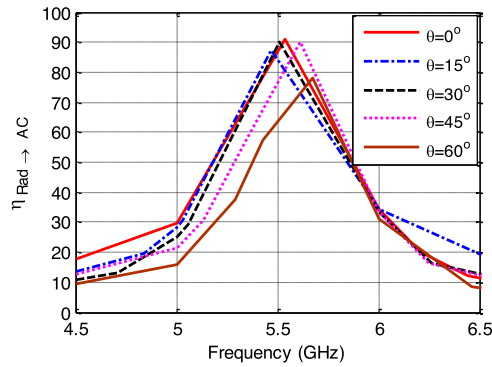**Figure 9.** Absorption ratio at different polarization angles.

Figure 10. The radiation to AC efficiency at different incident angles.

radiation to AC efficiency decreases as well as the operating frequency is slight shifted due to the changing in the direction of the incident EM waves.

3.2. Experimental and verification

The MS energy harvester was fabricated according to the specifications of the simulated array. Figure 11 depicts a 5×5 MS resonator array formed with a Rogers RO4350B substrate. All metallic vias are connected to individual surface-mount resistors (size 0603, Vishay), except the central unit cell, which is connected to the SMA connector. Figure 11(b) shows that the small gap between the via-pad and ground plane is filled with 50-Ω resistors. The central cell was chosen for measurement because it represents an infinite array in terms of simulation. The performance of the central unit cell represents the performance of other cells without edges.

To determine the power delivered to the central unit cell, the measurement setup suggested in [31, 32] is used. The experimental setup to determine the amount of power received by the MS harvester sample is shown Figure 12. The fabricated MS harvester sample is measured in the transmitter horn antenna's far-field region. To ensure that the harvester is excited by plane wave in the far-field region, the distance between the transmitter antenna and the MS harvester sample is calculated as follow
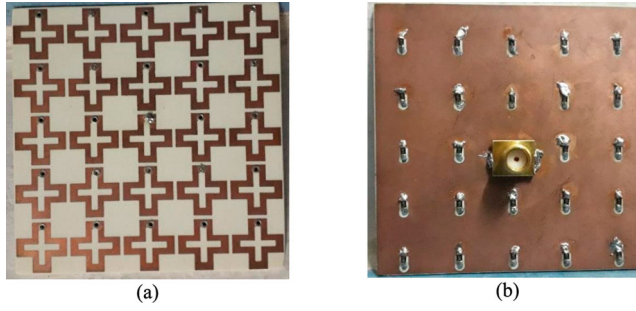
(a)   (b)

Figure 11. Fabricated MS harvester array; (a) Top view and (b) bottom view.
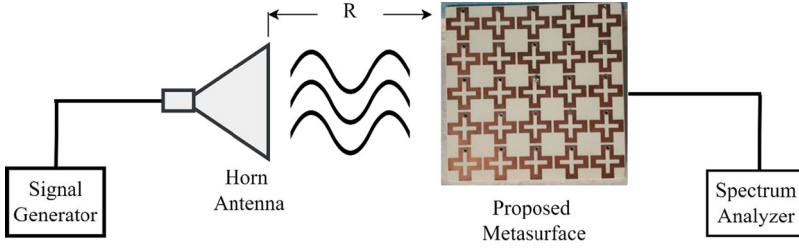

Figure 12. Experiment setup for measuring harvesting power efficiency of the proposed MS harvester.

$$R > \frac{2D^2}{\lambda} \qquad (5)$$

where R is the minimum distance between transmitting antenna and proposed metasurface harvester in (meter), D is the maximum dimension of the antenna in (meter) and λ is the wavelength in (meter). The horn antenna (type HF906) is fed with a 5 dBm signal from an Agilent Technologies CXA signal generator. The MS harvester sample is connected to an Agilent Technologies E8267D spectrum analyzer to determine the amount of power delivered to the central cell. The connectors, antenna, and cable losses are all considered while calibrating the measurement setup.

The harvesting efficiency of the MS harvester can be calculated using Equation (1), where the incident power on the MS harvester's footprint can be described as follows

$$P_{incident} = \frac{G_t P_t}{4\pi R^2} \times A_{(eff,array)} \qquad (6)$$

where, P_t is the horn antenna's input power when excited by a signal generator at a 5 dBm power level, G is the horn antenna's gain, and R is the distance between the horn antenna and the MS harvester which is R = 31 cm. Furthermore, $A_{(eff,array)} = 25\ A_{eff}$ is the array's effective area, which is equal to the number of unit cells, and A_{eff} is the central unit cell's effective area [33]. Figure 13 shows the measured power conversion efficiency as a function of frequency at different incident angles from 0° up to 60°. For incident angle of $\theta = 0^o$, the harvesting efficiency of about 82% is achieved at the 5.54 GHz. When the incident angles increased to $\theta = 30^o$ and $\theta = 60^o$, the harvesting efficiencies of about 75% and 67% are achieved at 5.5 and 5.65 GHz, respectively, as shown in Figure 13. Obviously, the proposed
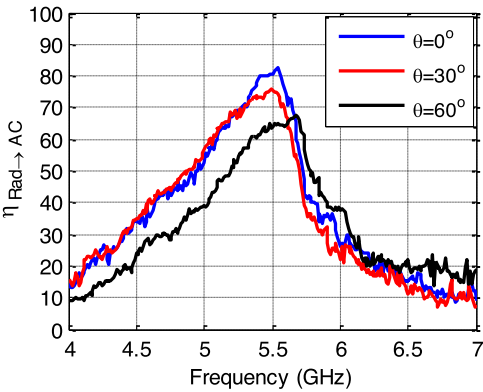
Figure 13. Measured radiation to AC conversion efficiency at different incident angles.

Table 1. Comparison of the unit cell's size and maximum harvesting efficiency across a wide range incident angle.

Ref. No	Size of structure	Substrate material	Center frequency	Incident angle range	Efficiency at 0°	Efficiency at 60°
[18]	$0.3\lambda_o$	Rogers Duroid RT5880	5.8	Normal incident	92%	Non
[19]	$0.34\lambda_o$	Rogers Duroid RT5880	5.55	Normal incident	83%	Non
[22]	$0.29\lambda_o$	–	5.8	0–75°	91%	72%
[34]	$0.6\lambda_o$	Rogers Duroid RT5880	5.4	0–60°	92%	50%
[35]	$0.32\lambda_o$	–	5.8	0–75°	88%	62%
This work	$0.22\lambda_o$	Rogers RO4350B	5.54	0–60°	91%	78.2%

MS structure performs well at different oblique incidence. There are three reasons for the discrepancy between the simulated and measured results. First, when it comes to fabricating a metasurface array, it is 5×5 whereas it is infinite in the simulation. The performance of the central cell will be influenced by the finite array's edge effect. Second, by setting the period boundary condition around the unit cell, the CST simulation software imitates an infinite array, which could lead to discrepancies with an actual infinite array. Third, the tolerances in the manufacturing process can also lead to errors. A reasonable agreement between the measurement and simulated results shows that the proposed MS harvester exhibits a wide-angle reception property.

Table 1 compares the proposed MS harvester and previous published papers in terms of a unit cell size, incident angle range, and the maximum harvesting efficiency at a normal incidence and an 60° oblique incidence angle. In comparison to previously published MS harvesters, the proposed MS is miniaturized, low cost and has a higher efficiency across a wider oblique incidence.

4. Conclusion

A wideband MS unit cell has been presented and demonstrated for ambient RFEH applications. An extensive numerical analysis of the MS structure was carried out using CST Microwave Studio, demonstrating a higher absorption ratio, good angular stability, and higher radiation to AC conversion efficiency within the 5.54 GHz frequency band. The

simulation results demonstrate that the proposed MS structure can efficiently capture EM power at a wide range of incident angles and deliver the maximum power of more than 78% to the load. A finite array unit cell is fabricated to verify the design, with all unit cells terminated by an optimal load resistance that matches the measurement tool impedance. The measured results agree well with the simulation. The proposed MS design incorporates advancements such as miniaturization, wide-angle reception, and higher conversion efficiency, making it ideal for ambient RFEH.

Acknowledgement

Disclosure statement

No potential conflict of interest was reported by the author(s).

ORCID

Abdulrahman Ahmed Ghaleb Amer 🔟 http://orcid.org/0000-0002-5997-0517

References

[1] Zhang H, Guo YX, Zhong Z, et al. Cooperative integration of RF energy harvesting and dedicated WPT for wireless sensor networks. IEEE Microw. Wirel. Components Lett. 2019;29(4):291–293.

[2] Shafique K, Khawaja B, Khurram M, et al. Energy harvesting using a Low-cost rectenna for internet of things (IoT) applications. IEEE Access. 2018;6:30932–30941.

[3] Song M, Belov P, Kapitanova P. Wireless power transfer inspired by the modern trends in electromagnetics. Appl. Phys. Rev. 2017;4(2):021102.

[4] Kim DS, Tran-Dang H. Wireless sensor networks for industrial applications. *SAS 2009 - IEEE Sensors Applications Symposium Proceedings*. 2019:127–140.

[5] Abdulkarem M, Samsudin K, Rokhani FZ, et al. Wireless sensor network for structural health monitoring: A contemporary review of technologies, challenges, and future direction. Struct. Heal. Monit. 2020;19(3):693–735.

[6] Belghith A, Obaidat MS. Wireless sensor networks applications to smart homes and cities. Vol. 1. In: Smart Cities and Homes. Elsevier Inc; 2016. p. 17–40.

[7] Yang XX, Jiang C, Elsherbeni AZ, et al. A novel compact printed rectenna for data communication systems. IEEE Trans. Antennas Propag. 2013;61(5):2532–2539.

[8] Shen S, Chiu CY, Murch RD. Multiport pixel rectenna for ambient RF energy harvesting. IEEE Trans. Antennas Propag. 2018;66(2):644–656.

[9] Sun H, Huang J, Wang Y. An omnidirectional rectenna array with an enhanced RF power distributing strategy for RF energy harvesting. IEEE Trans. Antennas Propag. 2022;70(6):4931–4936.

[10] Takabayashi N, Kawai K, Mase M, et al. Large-scale sequentially-fed array antenna radiating flat-Top beam for microwave power transmission to drones. IEEE J. Microwaves. 2022;2(2):297–306.

[11] Amer AAG, Sapuan SZ, Nasimuddin N, et al. Metasurface with wide-angle reception for electromagnetic energy harvesting. In: Proceedings of the 11th National Technical Seminar on Unmanned System Technology 2019. Lecture Notes in Electrical Engineering. 2021;666:693–700.

[12] Amer AAG, Sapuan SZ, Nasimuddin N, et al. A comprehensive review of metasurface structures suitable for RF energy harvesting. IEEE Access. 2020;8:76433–76452.

[13] Amer AAG, Sapuan SZ, Nasimuddin N, et al. A broadband wide-angle metasurface absorber for energy harvesting applications. Int. Conf. Technol. Sci. Adm. ICTSA 2021. 2021;1: 1–4.

[14] Amer AAG, Sapuan SZ, Alzahrani A, et al. Design and analysis of polarization-independent, wide-angle, broadband metasurface absorber using resistor-loaded split-ring resonators. Electronics. 2022;11(13):1986.

[15] Fang ZH, Chen H, An D, et al. Manipulation of visible-light polarization with dendritic cell-cluster metasurfaces. Sci. Rep. 2018;8(1):1–7.

[16] Li A, Singh S, Sievenpiper D. Metasurfaces and their applications. Nanophotonics. 2018;7(6):989–1011.

[17] Ramahi OM, Almoneef TS, AlShareef M, et al. Metamaterial particles for electromagnetic energy harvesting. Appl. Phys. Lett. 2012;101(17):173903.

[18] Alavikia B, Almoneef TS, Ramahi OM. Electromagnetic energy harvesting using complementary split-ring resonators. Appl. Phys. Lett. 2014;104(16):163903.

[19] Alavikia B, Almoneef TS, Ramahi OM. Complementary split ring resonator arrays for electromagnetic energy harvesting. Appl. Phys. Lett. 2015;107(3):033902.

[20] Amer AAG, Sapuan SZ, Nasimuddin N. Wide-coverage suspended metasurface energy harvester for ISM band applications. 2021 *IEEE 19th Student Conference on Research and Development (SCOReD)*. 2021:87–90.

[21] Ghaneizadeh A, Mafinezhad K, Joodaki M. Design and fabrication of a 2D-isotropic flexible ultra-thin metasurface for ambient electromagnetic energy harvesting. AIP Adv. 2019;9(2):025304.

[22] Yu F, He GQ, Yang XX, et al. Polarization-insensitive metasurface for harvesting electromagnetic energy with high efficiency and frequency stability over wide range of incidence angles. Appl. Sci. 2020;10(22):1–10.

[23] Ghaderi B, Nayyeri V, Soleimani M, et al. Pixelated metasurface for dual-band and multi-polarization electromagnetic energy harvesting. *Sci. Rep.* 2018;8(1): 13227.

[24] Karakaya E, Bagci F, Yilmaz AE, et al. Metamaterial-based four-band electromagnetic energy harvesting at commonly used GSM and Wi-Fi frequencies. J. Electron. Mater. 2019;48(4):2307–2316.

[25] DInh M, Ha-Van N, Tung NT, et al. Dual-polarized wide-angle energy harvester for self-powered IoT devices. IEEE Access. 2021;9:103376–103384.

[26] Aldhaeebi MA, Almoneef TS. Planar dual polarized metasurface array for microwave energy harvesting. Electron. 2020;9(12):1–13.

[27] Ghaderi B, Nayyeri V, Soleimani M, et al. Multi-polarisation electromagnetic energy harvesting with high efficiency. IET Microwaves, Antennas Propag. 2018;12(15):2271–2275.

[28] Costanzo S, Venneri F. Polarization-Insensitive fractal metamaterial surface for energy harvesting in IoT applications. Electronics. 2020;9(6):959.

[29] Luukkonen O, Costa F, Simovski CR, et al. A thin electromagnetic absorber for wide incidence angles and both polarizations. IEEE Trans. Antennas Propag. 2009;57(10):3119–3125.

[30] Bowen PT, Baron A, Smith DR. Theory of patch-antenna metamaterial perfect absorbers. Phys. Rev. A. 2016;93(6):063849.

[31] Hu W, Yang Z, Zaho F, et al. . Low-cost air gap metasurface structure for high absorption efficiency energy harvesting. Int. J. Antennas Propag. 2019;2019:1–8.

[32] Ghaneizadeh A, Joodaki M, Borcsok J, et al. Analysis, design, and implementation of a new extremely ultrathin 2-D-isotropic flexible energy harvester using symmetric patch FSS. IEEE Trans. Microw. Theory Tech. 2018;68(6):2108–2115.

[33] Younesiraad H, Bemani M. Broadband polarisation-independent metasurface electromagnetic energy harvester with high capture efficiency. IET Microwaves, Antennas Propag. 2020;14(13):1530–1536.

[34] Zhong H, Yang X. Broadband meta-surface with polarization-insensitive and wide-angle for electromagnetic energy harvesting. 2017 *International Workshop on Antenna Technology: Small Antennas, Innovative Structures, and Applications (iWAT)*. 2017:125–128.

[35] Yu F, Yang X, Zhong H, et al. Polarization-insensitive wide-angle-reception metasurface with simplified structure for harvesting electromagnetic energy. Appl. Phys. Lett. 2018;113(12):123903.